JACS
JOURNAL OF THE AMERICAN CHEMICAL SOCIETY

ARTICLE

pubs.acs.org/JACS

Synthesis and Morphogenesis of Organic Polymer Materials with Hierarchical Structures in Biominerals

Yuya Oaki,* Misako Kijima, and Hiroaki Imai*

Department of Applied Chemistry, Faculty of Science and Technology, Keio University, 3-14-1 Hiyoshi, Kohoku-ku, Yokohama 223-8522, Japan

Supporting Information

ABSTRACT: Synthesis and morphogenesis of polypyrrole (PPy) with hierarchical structures from nanoscopic to macroscopic scales have been achieved by using hierarchically organized architectures of biominerals. We adopted biominerals, such as a sea urchin spine and nacreous layer, having hierarchical architectures based on mesocrystals as model materials used for synthesis of an organic polymer. A sea urchin spine led to the formation of PPy macroscopic sponge structures consisting of nanosheets less than 100 nm in thickness with the mosaic interior of the nanoparticles. The morphologies of the resultant PPy hierarchical architectures can be tuned by the structural modification of the original biomineral with chemical and thermal treatments. In another case, a nacreous layer provided PPy porous nanosheets consisting of the nanoparticles. Conductive pathways were formed in these PPy hierarchical architectures. The nanoscale interspaces in the mesocrystal structures of biominerals are used for introduction and polymerization of the monomers, leading to the formation of hierarchically organized polymer architectures. These results show that functional organic materials with complex and nanoscale morphologies can be synthesized by using hierarchically organized architectures as observed in biominerals.

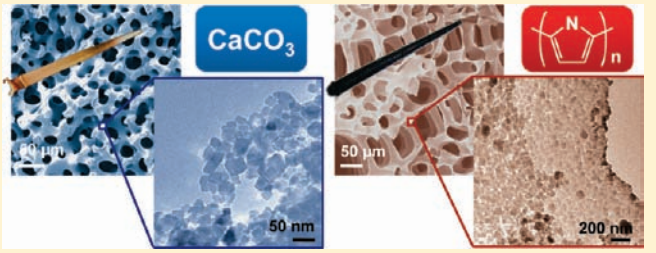

INTRODUCTION

Biominerals are inorganic/organic composites consisting of abundant minerals with hierarchically organized structures from nanoscopic to macroscopic scales.[1,2] In nature, controlled hierarchical structures of biominerals lead to a variety of functions such as mechanical and optical properties that are not conceivable from the components.[2] The biogenic functional hierarchical structures from nanoscopic to macroscopic scales can be used for synthesis and morphogenesis of other materials. Here we have obtained the hierarchical architectures of polypyrrole (PPy), a conductive polymer, by using hierarchically organized materials such as sea urchin spine and nacreous layer. The structure of oriented nanocrystals, namely mesocrystals, in the original materials plays important roles in the synthesis and morphogenesis of the PPy architectures.

Structures and formation processes of biominerals have attracted much interest as models in materials science.[3] Our group has found oriented nanocrystals with biological macromolecules, mesocrystals, in a variety of biominerals.[4,5] For example, nacreous layer and sea urchin exoskeleton have mesocrystal structures consisting of oriented calcium carbonate ($CaCO_3$) nanocrystals with incorporation of biological macromolecules. In biomineralization, biological macromolecules involve the control of crystal growth and morphogenesis leading to the formation of hierarchical structures based on mesocrystals. Inspired by biomineralization, biomimetic approaches for control of crystal growth have been widely studied with the assistance of organic molecules under mild conditions.

Our next challenge here is the synthesis and morphogenesis of organic polymer materials with hierarchically organized structures. In the present study, we have adopted two biominerals as the models for the syntheses of hierarchically organized polymer materials. The approach in the present study is to use a nanospace as the interspace in mesocrystals. The original biological polymers are removed from the mesocrystal structures of biominerals. Then, the introduction and polymerization of pyrrole (Py) monomers are performed in the nanospace. If the organic polymers can be synthesized in the $CaCO_3$ hierarchical structures of biominerals, the original carbonate crystals can be dissolved by chelating agents and dilute acids after the formation of polymer architectures. As for inorganic crystals, macroporous objects were fabricated by using the skeletal plates of a sea urchin spine, diatoms, and other biological architectures.[6−10] In earlier works, macroporous materials were obtained as the inverse structures of the original materials. There are no reports on the methodology for synthesis and morphogenesis of organic polymer materials by using the nanospace in mesocrystals. In addition to the macroscopic morphologies of biominerals, we focused on potentials of the nanostructures for synthesis and morphogenesis of a variety of materials, such as organic polymers, preserving hierarchically organized structures. Therefore, biominerals having hierarchically organized structures based on mesocrystals can be regarded as good models.

Received: January 6, 2011
Published: May 06, 2011

dx.doi.org/10.1021/ja200149u | J. Am. Chem. Soc. 2011, 133, 8594–8599

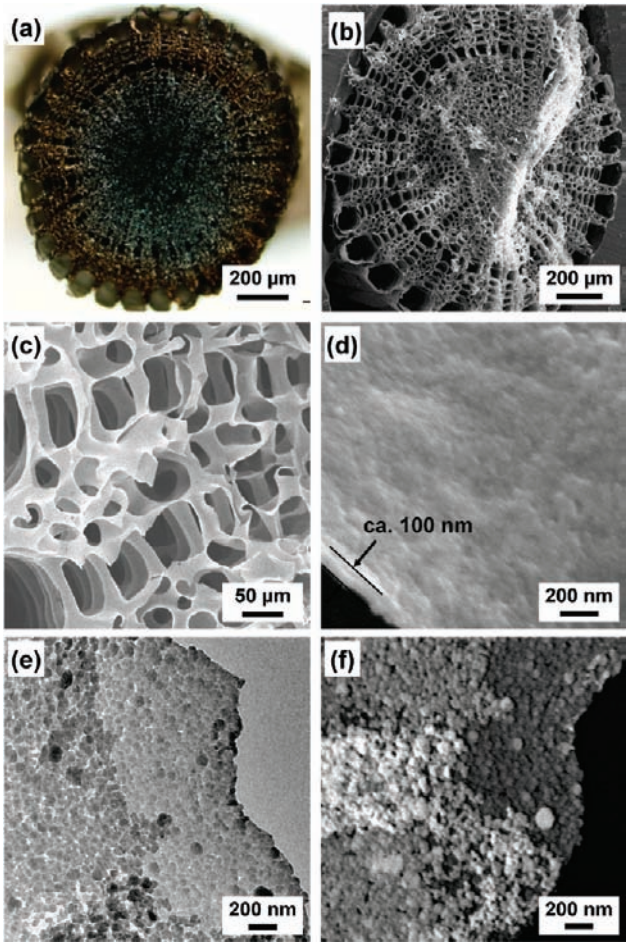

Figure 1. PPy hierarchical architectures synthesized from a sea urchin spine after dissolution of the $CaCO_3$ crystal and subsequent freeze–drying: (a) cross-sectional view of the spine consisting of PPy (optical microscope image); (b) FESEM image of the macroscopic sponge structures; (c, d) the magnified FESEM images of the sponge structure consisting of the nanosheets; (e, f) FETEM image and dark-field STEM image (white objects in black background) of the PPy sheets, respectively.

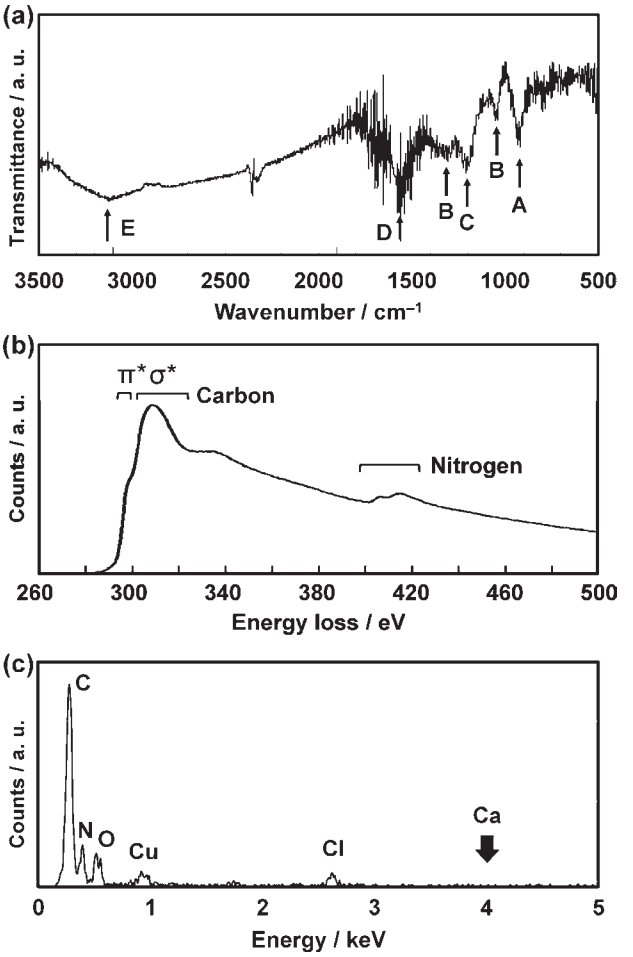

Figure 2. FT-IR spectrum (a), EELS analysis (b), and EDX analysis (c) of the PPy hierarchical architecture formed with a sea urchin spine after dissolution of $CaCO_3$: (a) absorption peaks assigned to the stretching vibrations of C═C and C–N bonds (A), in-plane and out-plane bending vibrations of the C–H bond (B), stretching vibrations of C–N and C–C bonds (C), in-ring stretching vibrations of C═C and C–C in the pyrrole rings and stretching vibrations of C═C and C–N bonds (D), and stretching vibrations of N–H and C–H bonds (E);[16c,21] (b) energy losses corresponding to the π^* and σ^* bands of carbon around 300 eV and the K-edge of nitrogen around 410 eV; (c) peaks assigned to carbon (C), nitrogen (N), oxygen (O), copper (Cu), and chloride (Cl). The peaks of calcium (Ca) originating from $CaCO_3$ disappeared. The appearance of a copper (Cu) peak was mainly caused by the Cu grid for FETEM observation (c).

In the present work, we have obtained hierarchical architectures of PPy from nanoscopic to macroscopic scales by using biominerals such as a sea urchin exoskeleton and nacreous layer. The PPy sponge structures consisting of nanosheets less than 100 nm in thickness were synthesized by the polymerization in the exoskeleton of a sea urchin spine. The nanosheets were comprised of PPy nanoparticles less than 50 nm in size. The thickness of the nanosheets involving the density of the sponge morphologies was controlled by the appropriate thermal treatments in the original biominerals. In addition, porous PPy nanosheets consisting of the nanoparticles were fabricated in the interspace between the aragonite plates of a nacreous layer. While morphologies of inorganic materials can be controlled through crystal growth, it is not so easy to tune morphologies of organic polymers through polymerization processes. If we can prepare the organic polymer materials by using the interspace in the carbonate-based mesocrystals, a wide variety of morphologies can be designed through the approach in the present work. A new rational approach to achieve the synthesis and morphogenesis of organic polymers will be an important technology.

Organic polymers with low-dimensional nanostructures and hierarchical architectures have attracted much interest.[11−15] In previous works,[11−15] functional organic polymers with nanostructures have been synthesized in confined spaces such as layered inorganic compounds, metal–organic frameworks, zeolites, and mesoporous materials. As for PPy, the surface coatings on substrates were performed by chemical and electrochemical deposition methods.[16] One-dimensional nanostructures were synthesized through template-assisted and template-free processes.[17,18] Two-dimensional (2D) network structures consisting of PPy nanowires were fabricated by using surfactants.[19] The stacks of 2D PPy nanostructures were synthesized in the redox-active coordination polymer.[20] However, it is not easy to synthesize controlled nanostructures including nanosheets and

dx.doi.org/10.1021/ja200149u | J. Am. Chem. Soc. 2011, 133, 8594–8599

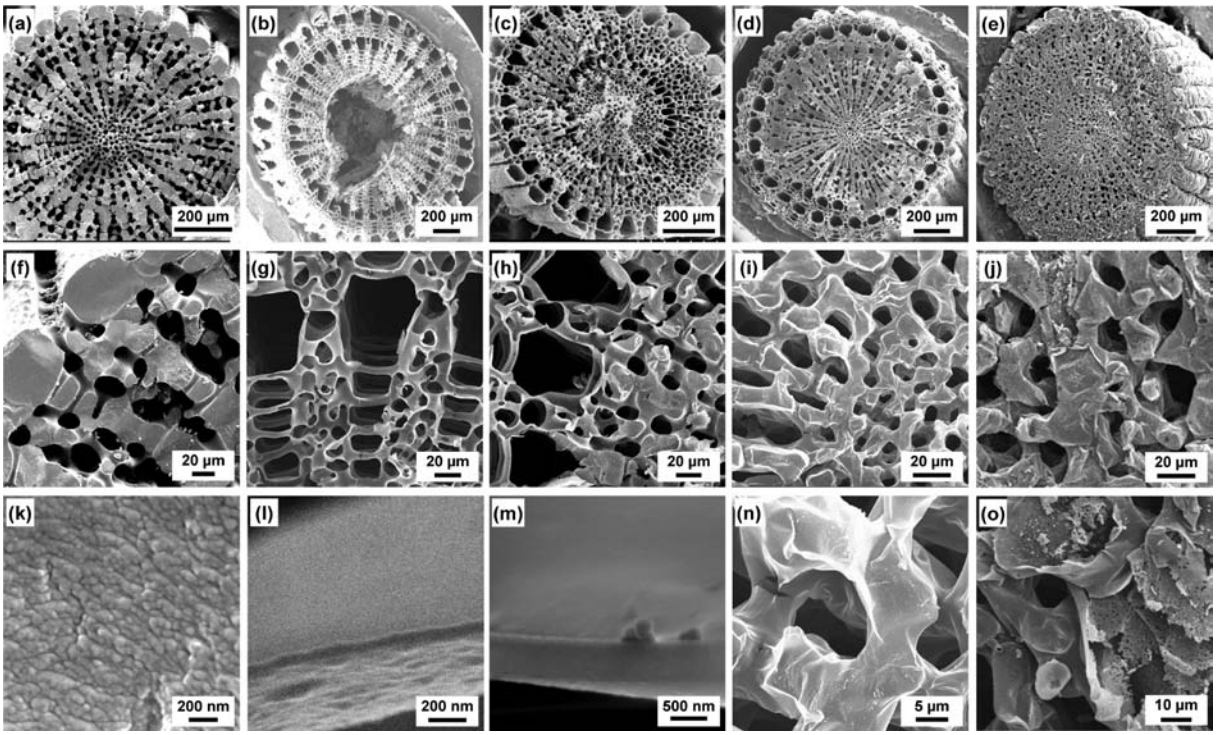

Figure 3. FESEM images of the original $CaCO_3$ sponge structures (a, f, k) and the PPy hierarchical architectures prepared from the original $CaCO_3$ sponge structures with no treatments (b, g, l), calcination at 450 °C for 2 h (c, h, m), calcination at 450 °C for 4 h (d, i, n), and 450 °C for 12 h (e, j, o): (a−e) cross-sectional views of the spine; (f−j) sponge structures; (k−o) magnified images of the walls in the sponge structures.

their hierarchically organized architectures. Conductive polymer materials with controlled nanostructures and morphologies can be used for a variety of nanoscale devices such as sensors and actuators.

RESULTS AND DISCUSSION

PPy Hierarchical Structure Based on Sea Urchin Spine. The exoskeleton of sea urchin spine treated with sodium hypochlorate (NaClO) aqueous solution was immersed in Py neat liquid. After the collection of the specimen, the excess Py liquid was absorbed by a paper towel. Before further drying, the Py-included samples were maintained in 2-propanol (2-PrOH) containing 100 mM of copper chloride ($CuCl_2$). The hierarchical structures of PPy were obtained after the dissolution of $CaCO_3$ crystals and subsequent freeze−drying (Figure 1). The macroscopic sponge structure has a black color, and the continuous pores are 10−50 μm in size (Figure 1a−c). The sponge structure consisted of nanosheets 50−100 nm in thickness (Figure 1c,d). Densely packed nanoparticles 20−50 nm in size were observed inside the sheets (Figure 1e,f). The FT-IR and EELS analyses indicate the formation of PPy (Figure 2a,b). The absorption bands are assigned to stretching vibrations of C═C and C−N bonds (A), in-plane and out-of-plane bending vibrations of the C−H bond (B), in-ring stretching vibrations of C═C and C−C bonds in the pyrrole rings and stretching vibrations of C═C and C−N bonds (D), and stretching vibrations of N−H and C−H bonds in the pyrrole rings (E) (Figure 2a). These absorptions are characteristic of those for PPy.[16c,21] The EELS spectrum shows the energy losses corresponding to K-edges of π^* and σ^* bands of carbon around 300 eV and the K-edge of nitrogen around 410 eV (Figure 2b). In addition, the remaining calcium ion originating from the original $CaCO_3$ mesocrystals was not detected in the EDX spectrum (Figure 2c). The peaks of carbon, nitrogen, oxygen, and chloride only appeared in the EDX spectrum. The appearance of a chloride peak implies the doping from $CuCl_2$ used for the polymerization. On the basis of these results, we successfully synthesized PPy hierarchically organized structures from nanoscopic to macroscopic scales by using biominerals in the solution processes at room temperature.

Morphological Variation of the PPy Architectures. Interestingly, the morphologies of the PPy hierarchical structures can be tuned by the changes of the conditions for the treatments of the original exoskeletons prior to the introduction of Py monomers (Figure 3). The original $CaCO_3$ sponge structures based on the mesocrystal were shown in Figure 3a,f,k. When the original exoskeleton was not treated by NaClO, thinner PPy nanosheets ca. 50 nm in thickness consisting of nanoparticles made up the macroscopic sponge architectures (Figure 3b,g,l). The sea urchin spine treated at 450 °C for 2 h provided PPy sponge structures consisting of sheets thicker than 700 nm (Figure 3c,h,m). An increase in the thickness of the sheets led to the formation of a sponge structure with a dense skeleton (Figures 1d and 3g,h). As the time for the thermal treatment of original sea urchin spines was increased to 4 h, the resultant PPy showed sponge structures with a dense skeleton consisting of thicker sheets (Figure 3d,i,n). A further increase in the time for the thermal treatment to 12 h formed the dense skeleton of the sponge structures with the inside pores (Figure 3e,j,o). In this way, the changes of the structures in the original material led to the morphological evolution of the resultant PPy architectures.

Formation Mechanisms of the PPy Hierarchical Architectures. On the basis of these results, the morphogenesis of a variety of the PPy hierarchical architectures cannot be simply

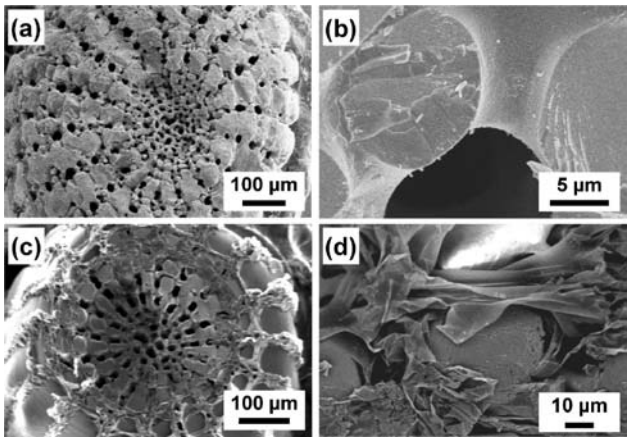

Figure 4. Formation processes of the PPy hierarchical architectures from a sea urchin spine: (a, b) composite structures of the original $CaCO_3$ skeletons and PPy after the introduction of Py and subsequent polymerization; (c, d) partial dissolution of $CaCO_3$ from the composite structures by EDTA-2Na, leading to the appearance of nanosheets.

ascribed to the formation of the macroscopic inverse sponge structures. After immersion in Py neat liquid, the Py monomer remaining in the macroscopic pore of the sea urchin spine was removed through absorption by a paper towel. Therefore, the Py monomer was confined in the $CaCO_3$ body of the spine. When the Py-included spine was immersed in a $CuCl_2$ aqueous solution, the color of the spine immediately changed to black. Since the black precipitates of PPy were not observed in the solution phase, the Py monomer was rapidly polymerized from the surface of the spine without elution into the solution phase. The polymerization proceeds in the body of the spine. After the polymerization of Py, the color of the spine changed from white to black (Figure 1a). Nevertheless, changes in the morphologies were not observed in the FESEM images after the incorporation and polymerization of Py (Figure 4). PPy was not filled in the macroscopic pores in the original sponge structures consisting of $CaCO_3$. The inverse structures of the original macroscopic sponge were not formed through the introduction and polymerization of Py. These results imply that Py monomer is introduced in the nanospace of the $CaCO_3$ mesocrystals. After polymerization, the nanocomposites of the original $CaCO_3$ mesocrystals and the resultant PPy are formed in the skeleton of sponge structures. Therefore, PPy sponge architectures consisting of the nanosheets appear from the composite structures after the dissolution of the $CaCO_3$ mesocrystal and subsequent freeze−drying (Figure 4c,d).

The interspace in the mesocrystal structures plays an important role in the synthesis and morphogenesis of the PPy hierarchical structures. When the micrometer-sized calcite $CaCO_3$ crystal without a mesocrystal structure was used as a control experiment, similar PPy hierarchical architectures were not obtained. The nanospace in the mesocrystal structures facilitates the incorporation of Py monomers in the original sponge structures. As noted in our previous reports,[4,5,22] organic molecules can be introduced in the interspace in the mesocrystal structures even before the removal of organic molecules by the NaClO treatment. In the present study, Py monomers are incorporated and confined in the interspace in the $CaCO_3$ mesocrystal structures through the immersion in Py neat liquid. The confined Py monomers in the nanospace are not eluted in 2-PrOH containing $CuCl_2$ for the polymerization. Then, the incorporated monomers are polymerized around the $CaCO_3$ nanocrystals in the mesocrystal structures. The PPy hierarchical structures appear after the dissolution of $CaCO_3$ and freeze−drying. In the PPy sponges, nanoparticles were formed (Figure 1e,f). The formation of PPy nanoparticles in the hierarchical architecture is ascribed to the polymerization method and/or the size of the nanospace.

The microscale morphologies of the resultant PPy sponge structures were tuned by the thermal treatments of the original sponge structures (Figures 3 and 5). On the basis of the TG analysis (Figure S2 in the Supporting Information), ca. 10 wt % of organic components was included in the original sponge structures consisting of calcite nanocrystals ca. 20 nm in size.[4,5] Since Py monomer does not fully penetrate into the skeleton of the original sponge structures, the polymerization of Py proceeds near the surface of the sponge structure (Figure 5b,g). Thin PPy nanosheets about 50 nm in thickness made up the replicated morphology of the original sponge structure (Figure 3b,g,l). After NaClO treatment of the sea urchin spine, the residual organic components decreased to about 1.3 wt % (Figure S2 in the Supporting Information). The decrease of the organic components provides more space for the introduction of Py monomers in the interspace in the mesocrystals (Figure 5c,h). The thicker PPy nanosheets (about 100 nm) led to the formation of a similar replicated sponge morphology (Figure 1). TG analysis suggests that most of the organic molecules in the original sponge structure can be removed by thermal treatment in air at 450 °C (Figure S2 in the Supporting Information). After thermal treatment at 450 °C for 2 and 4 h, the nanospace in the PPy sponge structure is increased through the removal of organic components (Figure 5c−e,h−j). In addition to the removal of the organic molecules, sintering and grain growth provide a larger nanospace for the introduction of the Py monomers (Figure 5g−j). Therefore, the Py monomers can be easily introduced inside the sponge skeleton. The thickening of the sheets constructed sponge morphologies with a dense skeleton, similar to those observed in the original species (Figure 3c,d,h,i,m,n). When the time of thermal treatment is prolonged to 12 h, the size of the $CaCO_3$ nanocrystals is increased through the sintering with grain growth. After the polymerization of Py, pores are formed in the skeleton of the PPy sponge by the dissolution of the large $CaCO_3$ crystals (Figure 3e, j,o). In this way, morphological tuning was achieved by changes of the structures in the skeletons of the original sponges through appropriate thermal treatments.

Conductivity Measurements. The electrical conduction of the resultant PPy architectures was confirmed by a two-probe method (Figure S1 in the Supporting Information). The conductivity of a resultant PPy hierarchical structure was estimated to be 3.06×10^{-6} S cm^{-1} without any doping. The conductivity increased to 2.52×10^{-4} S cm^{-1} after doping with iodide (I_2). The resultant PPy hierarchical architectures have a continuous conductive pass. In contrast, conduction could not be detected on a sea urchin spine without introduction of Py. Further analyses and the improvement of the conductivity are required.

PPy Hierarchical Structure Based on Nacreous Layer. We obtained the PPy 2D nanostructure in the nacreous layer (Figure 6). PPy nanostructures were prepared in the interspace of the layered aragonite plates after removal of the organic sheets. As noted in previous works,[4,5a] the layered structures are comprised of organic sheets ca. 20 nm in thickness and aragonite plates 200−800 nm in thickness. Moreover, nanocrystals 50−100 nm in size form the mesocrystal structures in each aragonite

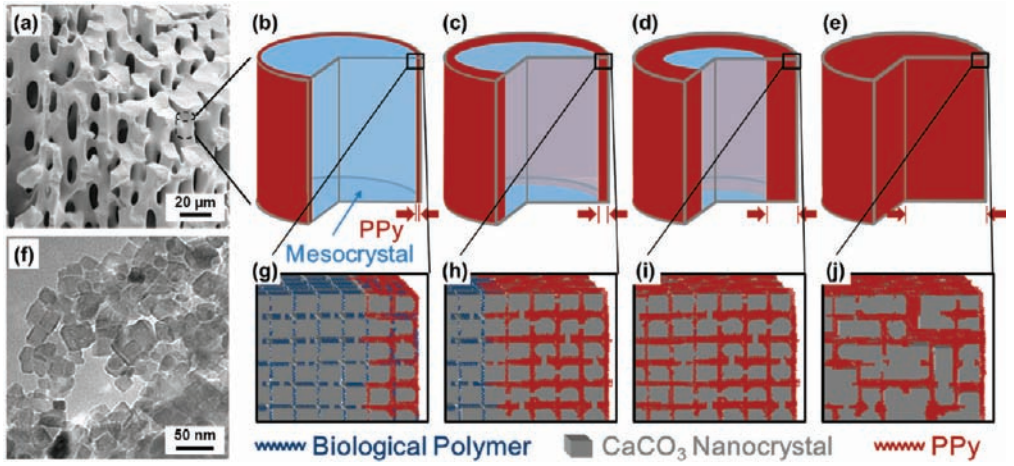

Figure 5. Schematic representations for the proposed formation mechanisms of the PPy hierarchical architectures: (a, f) FESEM and FETEM images of the original $CaCO_3$ sponge structure, respectively; (b−e, g−j) introduction behavior of Py in the skeletons of the $CaCO_3$ sponge structures with no treatment (b and g), calcination at 450 °C for 2 h (c and h), calcination at 450 °C for 4 h (d and i), and calcination at 450 °C for 12 h (e and j).

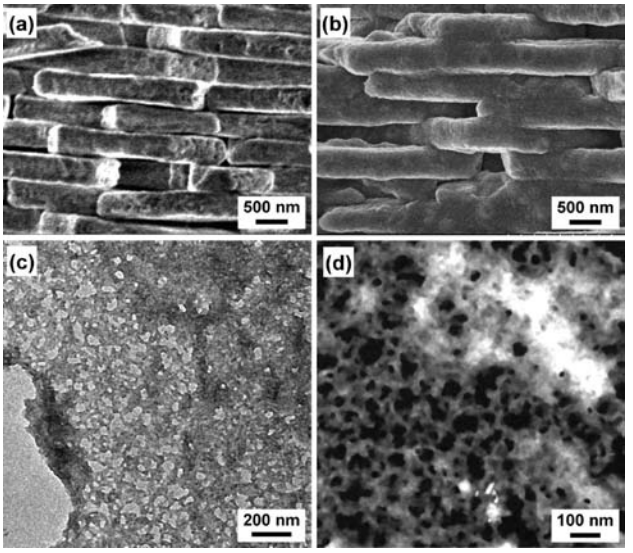

Figure 6. PPy hierarchical architectures synthesized from a nacreous layer: (a) layered structure of aragonite plates after thermal treatment for the removal of organic macromolecules; (b) FESEM images after the formation of PPy in the interlayer space of the aragonite plates; (c, d) FETEM and dark-field STEM images of the PPy nanostructures observed after the dissolution of the carbonates, respectively.

plate. We initially removed the organic sheets to generate the nanospace for introduction of Py monomers by calcination at 300 °C for 2 h.[23] Then, the introduction of the monomer and subsequent polymerization were performed by the same methods as those of the sea urchin spine.

After calcination, the interspace of the layered structures appeared on the FESEM images after the removal of the organic components (Figure 6a). TG analyses suggest that the organic components decreased from 4.0 to 2.4 wt % after the calcination (Figure S3 in the Supporting Information). The introduction of Py monomers and subsequent polymerization led to an increase in the organic contents to 3.3 wt %. The FESEM image shows that the polymerization induced the formation of PPy nanostructures between the aragonite plates (Figure 6b). The layered aragonite plates formed composites with the PPy instead of the original biological polymers (Figure 6a,b). When the aragonite plates were dissolved by EDTA-2Na, nanosheets with pores 20−50 nm in size were observed in the FETEM images (Figure 6c,d).[24] The macroscopic layered morphologies of the original nacreous layer were not preserved after the dissolution of the aragonite plates. EELS analysis supported the formation of PPy (Figure S4 in the Supporting Information). PPy was formed in the interspace of the aragonite plates and in the mesocrystal structure inside each aragonite plate through introduction of Py monomer and subsequent polymerization. As well as sea urchin spine, the nanospace in the mesocrystal structures facilitates the formation of PPy hierarchical structures.

The resultant PPy network formed in the nacreous layer showed electrical conduction on doping with I_2 from the vapor. The measurement of conductance was performed in the composite structures of the PPy and aragonite plates. The conductances parallel and perpendicular to the layered structure of nacre were 3.98×10^{-7} S and 2.17×10^{-6} S, respectively. The results suggest that the PPy networks generated continuous 2D nanostructures having electrical conduction in the composites.

■ CONCLUSIONS

We achieved the synthesis and morphogenesis of PPy hierarchical architectures by using hierarchically organized structures in biominerals such as sea urchin spine and nacreous layer. The PPy hierarchically organized structures include macroscopic sponge structures, nanosheets, and nanoparticles. Morphological tuning of the resultant PPy architectures was achieved by changes in the original mesocrystal structures. PPy porous nanosheets were formed in the interlayer space of the nacreous layer and in the interspace of the mesocrystals. In the present work, biominerals such as sea urchin spine and nacreous layer were not typical templates for the fabrication of the macroscopic inverted morphologies. The results indicate that the approach is not a hierarchical templating technique but a new methodology for morphogenesis based on mesocrystal structures. The mesocrystal structures in the biominerals facilitate the synthesis and morphogenesis of continuous PPy architectures with electric conduction. On the basis of the present results, a variety of

hierarchically organized materials based on mesocrystals can be used for the synthesis and morphogenesis of organic polymers by using the nanospace. The mesocrystals and confined organic polymers form the nanocomposites. If the original materials are dissolved after the polymerization, replicated polymer architectures can be obtained. Furthermore, the other functional organic polymers can be prepared by changes in the monomers and reaction conditions in a similar simple method. Further studies promise the emergence of new properties and development of functions.

■ ASSOCIATED CONTENT

Supporting Information. Text giving experimental details and figures giving detailed data, including conductivity measurements, TG, and EELS analyses. This material is available free of charge via the Internet at http://pubs.acs.org.

■ AUTHOR INFORMATION

Corresponding Author

*E-mail: oakiyuya@applc.keio.ac.jp (Y.O.); hiroaki@applc.keio.ac.jp (H.I.).

■ ACKNOWLEDGMENT

This work was partially supported by Grants-in-Aid for Scientific Research on Innovative Areas of "Fusion Materials: Creative Development of Materials and Exploration of Their Function through Molecular Control" (No. 2206) (H.I.) from the Ministry of Education, Culture, Sports, Science and Technology, for Young Scientist (A, No. 21850025) (Y.O.) from the Japan Society of the Promotion of Science, and for Research on Materials Processing Learning from Nature from Sekisui Chemical (Y.O.).

■ REFERENCES

(1) (a) Mann, S. *Nature* **1988**, *332*, 119. (b) Addadi, L.; Weiner, S. *Angew. Chem., Int. Ed. Engl.* **1992**, *31*, 153. (c) Stupp, S. I.; Braun, P. V. *Science* **1997**, *277*, 1242. (d) Mann, S. In *Biomineralization Principles and Concepts in Bioinorganic Materials Chemistry*; Compton, R. G., Davies, S. G., Evans, J. , Eds.; Oxford University Press: Oxford, U.K., 2001. (e) Sarikaya, M.; Tamerler, C.; Jen, A. K. Y.; Schulten, K.; Baneyx, F. *Nat. Mater.* **2003**, *2*, 577.

(2) (a) Jackson, A. P.; Vincent, J. F. V.; Turner, R. M. *Proc. R. Soc. London, Ser. B* **1988**, *234*, 415. (b) Aizenberg, J.; Tkachenko, A.; Weiner, S.; Addadi, L. *Nature* **2001**, *412*, 819. (c) Dorozhkin, S. V.; Epple, M. *Angew. Chem., Int. Ed.* **2002**, *41*, 3130. (d) Aizenberg, J.; Hendler, G. *J. Mater. Chem.* **2004**, *14*, 2066. (e) Bechtle, S.; Ang, S. F.; Schneider, G. A. *Biomaterials* **2010**, *31*, 6378. (f) Raabe, D.; Sachs, C.; Romano, P. *Acta Mater.* **2005**, *53*, 4281.

(3) (a) Mann, S. *Nature* **1993**, *365*, 499. (b) Kato, T. *Adv. Mater.* **2000**, *12*, 1543. (c) Yu, S.-H.; Cölfen, H. *J. Mater. Chem.* **2004**, *14*, 2124. (d) Imai, H.; Oaki, Y.; Kotachi, A. *Bull. Chem. Soc. Jpn.* **2006**, *79*, 1834. (e) Xu, A.-W.; Ma, Y.; Cölfen, H. *J. Mater. Chem.* **2007**, *17*, 415. (f) Estroff, L. A. *Chem. Rev.* **2008**, *108*, 4329. (g) Meldrum, F. C.; Cölfen, H. *Chem. Rev.* **2008**, *108*, 4332. (h) Sommerdijk, N. A. J. M.; de With, G. *Chem. Rev.* **2008**, *108*, 4499. (i) Gower, L. B. *Chem. Rev.* **2008**, *108*, 4551. (j) Mann, S. *Nat. Mater.* **2009**, *8*, 781. (k) Kato, T.; Sakamoto, T.; Nishimura, T. *MRS Bull.* **2010**, *35*, 127. (l) Imai, H.; Oaki, Y. *MRS Bull.* **2010**, *35*, 138.

(4) Oaki, Y.; Imai, H. *Angew. Chem., Int. Ed.* **2005**, *44*, 6571.

(5) (a) Oaki, Y.; Kotachi, A.; Miura, T.; Imai, H. *Adv. Funct. Mater.* **2006**, *16*, 1633. (b) Oaki, Y.; Imai, H. *Small* **2006**, *2*, 66.

(6) (a) Park, R. J.; Meldrum, F. C. *Adv. Mater.* **2002**, *14*, 1167. (b) Park, R. J.; Meldrum, F. C. *J. Mater. Chem.* **2004**, *14*, 2291. (c) Yue, W.; Kulak, A. N.; Meldrum, F. C. *J. Mater. Chem.* **2006**, *16*, 408. (d) Yue, W.; Park, R. J.; Kulak, A. N.; Meldrum, F. C. *J. Cryst. Growth* **2006**, *294*, 69. (e) Meldrum, F. C. *Macromol. Biosci.* **2007**, *7*, 152. (f) Lai, M.; Kulak, A. N.; Law, D.; Zhang, Z.; Meldrum, F. C.; Riley, D. J. *Chem. Commun.* **2007**, 3547.

(7) Ha, Y. H.; Vaia, R. A.; Lynn, W. F.; Costantino, J. P.; Shin, J.; Smith, A. B.; Matsudaira, P. T.; Thomas, E. L. *Adv. Mater.* **2004**, *16*, 1091.

(8) Cheng, X.; Gower, L. B. *Biotechnol. Prog.* **2006**, *22*, 141.

(9) (a) Gaddis, C. S.; Sandhage, K. H. *J. Mater. Res.* **2004**, *19*, 2541. (b) Kusari, U.; Bao, Z.; Cai, Y.; Ahmad, G.; Sandhage, K. H.; Sneddon, L. G. *Chem. Commun.* **2007**, 1177. (c) Bao, Z.; Ernst, E. M.; Yoo, S.; Sandhage, K. H. *Adv. Mater.* **2009**, *21*, 474. (d) Toster, J.; Lyer, K. S.; Burtovyy, R.; Burgess, S. S. O.; Luzinov, I. A.; Ratson, C. L. *J. Am. Chem. Soc.* **2009**, *131*, 8356. (e) Zhou, H.; Fan, T.; Li, X.; Ding, J.; Zhang, D.; Li, X.; Gao, Y. *Eur. J. Inorg. Chem.* **2009**, 211.

(10) (a) Hall, S. R.; Bolger, H.; Mann, S. *Chem. Commun.* **2003**, 2784. (b) Zhang, W.; Zhang, D.; Fan, T.; Gu, J.; Ding, J.; Wang, H.; Guo, Q.; Ogawa, H. *Chem. Mater.* **2009**, *21*, 33. (c) Zhao, Y.; Wei, M.; Lu, J.; Wang, Z. L.; Duan, X. *ACS Nano* **2009**, *3*, 4009. (d) Galusha, J. W.; Richey, L. R.; Jorgensen, M. R.; Gardner, J. S.; Bartl, M. H. *J. Mater. Chem.* **2010**, *20*, 1277.

(11) Ruiz-Hitzky, E. *Adv. Mater.* **1993**, *5*, 334.

(12) Tajima, K.; Aida, T. *Chem. Commun.* **2000**, 2399.

(13) Cardin, D. J. *Adv. Mater.* **2002**, *14*, 553.

(14) Tran, H. D.; Li, D.; Kaner, R. B. *Adv. Mater.* **2009**, *21*, 1487.

(15) (a) Wu, C. G.; Bein, T. *Science* **1994**, *264*, 1757. (b) Matsubara, I.; Hosono, K.; Maruyama, N.; Shin, W.; Izu, N. *Bull. Chem. Soc. Jpn.* **2004**, *77*, 1231. (c) Sozzani, P.; Bracco, S.; Comotti, A.; Simonutti, R.; Valsesia, P.; Sakamoto, Y.; Terasaki, O. *Nat. Mater.* **2006**, *5*, 545. (d) Lataïef, S.; Aranda, P.; Fernández-Saaverda, R.; Margeson, J. C.; Detellier, C.; Ruiz-Hitzky, E. *J. Mater. Chem.* **2008**, *18*, 2227.

(16) (a) Yoshino, K.; Hayashi, S.; Sugimoto, R. *Jpn. J. Appl. Phys.* **1984**, *23*, L899. (b) Bjorklund, R. B.; Landström, T. *J. Electron. Mater.* **1984**, *13*, 211. (c) Lu, Y.; Shi, G.; Li, C.; Liang, Y. *J. Appl. Polym. Sci.* **1998**, *70*, 2169. (d) Huang, J.; Ichinose, I.; Kunitake, T. *Chem. Commun.* **2005**, 1717–1719. (e) Lu, X.; Zhao, Q.; Li, X.; Wang, D.; Zhang, W.; Wang, C.; Wei, Y. *Macromol. Rapid Commun.* **2006**, *27*, 430. (f) Strandwitz, N. C.; Nonoguchi, Y.; Boettcher, S. W.; Stucky, G. D. *Langmuir* **2010**, *26*, 5319.

(17) (a) Hatano, T.; Takeuchi, M.; Ikeda, A.; Shinkai, S. *Org. Lett.* **2003**, *5*, 1395. (b) Bae, A. H.; Hatano, T.; Numata, M.; Takeuchi, M.; Shinkai, S. *Macromolecules* **2005**, *38*, 1609.

(18) (a) Zhang, X.; Zhang, J.; Lin, Z.; Robinson, C. *Chem. Commun.* **2004**, 1852. (b) Tran, H. D.; Shin, K.; Hong, W. G.; D'Arcy, J. M.; Kojima, R.; Weiller, B. H.; Kaner, R. B. *Macromol. Rapid Commun.* **2007**, *28*, 2289.

(19) (a) Wu, A.; Kolla, H.; Manohar, S. K. *Macromolecules* **2005**, *38*, 7873. (b) Zhong, W.; Liu, S.; Chen, X.; Wang, Y.; Yang, W. *Macromolecules* **2006**, *39*, 3224. (c) Feng, J.; Yan, W.; Zhu, J. *Synth. Met.* **2010**, *160*, 939.

(20) Yanai, N.; Uemura, T.; Ohba, M.; Kadowaki, Y.; Maesato, M.; Takenaka, M.; Nishitsuji, S.; Hasegawa, H.; Kitagawa, S. *Angew. Chem., Int. Ed.* **2008**, *47*, 9883.

(21) Kostić, R.; Raković, D.; Stepanyan, S. A.; Davidova, I. E.; Gribov, L. A. *J. Chem. Phys.* **1995**, *102*, 3104.

(22) (a) Oaki, Y.; Imai, H. *Adv. Funct. Mater.* **2005**, *15*, 1407. (b) Oaki, Y.; Imai, H. *Chem. Commun.* **2005**, 6011. (c) Oaki, Y.; Imai, H. *Bull. Chem. Soc. Jpn.* **2009**, *82*, 613.

(23) When the nacreous layer was immersed in NaClO aqueous solution to remove the organic macromolecules, the Py monomer was not introduced in the interspace even after NaClO treatment.

(24) On the basis of the TG analyses (Figures S2 and S3 in the Supporting Information), the original biological macromolecules may remain in the resultant composites of the nacreous layer and PPy architectures. However, it is inferred that the remaining biological macromolecules are dissolved and/or removed with the original $CaCO_3$ crystals through the dissolution process by using EDTA-2Na.